The shapes of dikes: Evidence for the influence of cooling and inelastic deformation

Katherine A. Daniels, Janine Kavanagh, Thierry Menand, R.S.J. Sparks

The shapes of dikes: evidence for the influence of cooling and inelastic deformation.

Katherine A. Daniels[1], Janine L. Kavanagh[2], Thierry Menand[3,4,5] and R. Stephen J. Sparks[1].

[1]School of Earth Sciences, University of Bristol, Wills Memorial Building, Queen's Road, Bristol, BS8 1RJ, U.K.

[2]School of Geosciences, Monash University, Clayton Campus, Wellington Road, Clayton, Victoria, 3800, Australia.

[3]Clermont Université, Université Blaise Pascal, Laboratoire Magmas et Volcans, BP 10448, F-63000 Clermont-Ferrand, France.

[4]CNRS, UMR 6524, LMV, F-63038 Clermont-Ferrand, France.

[5]IRD, R 163, LMV, F-63038 Clermont-Ferrand, France.

Abstract

We document the shape of dikes from well exposed field locations in the Isle of Rum, Scotland, and Helam Mine, South Africa. The basaltic Rum dikes crop out on a smaller scale than the Helam kimberlite dikes and have a smaller length to thickness ratio (~100:1 Isle of Rum, ~1000:1 Helam Mine). We compare dike thickness field measurements with the geometry predicted by elastic theory, finding best-fit models to estimate magma overpressure and regional stress gradients at the time of dike emplacement. Most of the dike shapes fit poorly with elastic theory, being too thick at the dike ends and too narrow in the middle. Our calculated overpressures and stress gradients are much larger than independent estimates based on rock strength. Dike shape can be explained by a combination of host rock inelastic deformation and magma chilling at the dike's tapering edges preventing its closure as magma pressure declines

during emplacement. The permanent wedging of the dike edges due to chilling has implications for crustal magma transport and strain response in the crust due to dike emplacement.

1. Introduction

Dikes are the end result of the flow of pressurised magma through fractures, recording a fundamental mechanism of magma transport through the crust. Dike shapes reflect the integration of complex emplacement and eruption processes, where host-rock deformation, magma viscosity, magma pressure variations, stress distribution and heat transfer all play a role. Many theoretical and experimental studies of dike emplacement emphasize elastic deformation by pressurised magma-filled fractures (e.g. Gudmundsson 1983, Lister and Kerr 1991, Kerr and Lister 1995, Rubin 1995, Menand and Tait 2001, Menand and Tait 2002, Ray et al. 2007, Menand et al. 2010).

The shape of a preserved solidified dike can be used to calculate the pressure in the crack at the time of solidification, assuming that the shape reflects a simple elastic deformation control with fixed overpressure. Previous studies of dike shape have involved the measurement of dike thicknesses in the field and the observed dike cross-sectional profiles have been compared with elastic models in order to estimate the driving pressures and stress gradients at the time of emplacement (Pollard and Muller 1976, Delaney and Pollard 1981, Rubin and Pollard 1987, Poland et al. 2008, Geshi et al. 2010, Kavanagh and Sparks, 2011). Others have used theoretical numerical models to interpret the evolution of dike thickness. Buck et al. (2006) found that the stopping pressure of a dike (the point where the difference between the magma pressure and the tectonic stress (the driving pressure) at the dike tip becomes too small to propagate the dike) is

proportional to its thickness. They also found that the propagation distance is dependent on the initial distribution of tectonic stress and that dike intrusions affect the tectonic stress distribution, therefore affecting the propagation of subsequent dikes. Gudmundsson (2011) suggests that dike arrest is dependent on a number of factors including the size of the process zone (a region of highly fractured host-rock formed ahead of the propagating intrusion (see, for example, White et al., 2011)), in addition to the fracture toughness of both the host-rock itself and the interfaces between rock units. As a consequence, two dikes with the same overpressure could have quite different thicknesses.

We document the shapes of well exposed examples of basaltic dikes from the Isle of Rum, Scotland, and kimberlite dikes from Helam Mine, South Africa. Firstly we describe the geological settings of the dikes and present detailed dike-thickness datasets. We then summarize the theoretical framework used to assess to what extent elastic deformation can describe dike shape. We find that the shapes of most of the dikes have a poor fit with that expected from elastic theory and propose that the shapes can be explained by including the complicating effects of magma chilling at the dike's tapering edges and host-rock inelastic deformation.

Our observations have implications for understanding the development of dikes as conduits and for the effects of dikes on transient stresses and crustal strain. Through the permanent wedging open of the crust by chilled dike edges, a dike can act as a potential conduit for longer, increasing the longevity of eruptions. In addition the crustal strains implicit in dike emplacement reflect not only responses to tectonic stress but also magma overpressures preserved at the dike edges by chilling.

2. Geological settings

Basaltic dikes from the Isle of Rum

Situated off the west coast of Scotland, the Isle of Rum represents the eroded remnants of a shallow-level igneous complex emplaced into Torridonian Pre-Cambrian sandstone at approximately 2-3 km depth (e.g. Emeleus 1997, Nichols et al. 2009). Rum's igneous rocks include layered basic and ultrabasic intrusions, granophyres, volcanic rocks ranging from rhyolite to picrite, and hypabyssal intrusions (Emeleus 1997). The focus of this study is a late stage NW- to NNW-striking basaltic dike swarm (Emeleus 1997) dated to 60.53 ± 0.08 Ma (Hamilton et al. 1998). The Isle of Rum and the dike measurement locations are shown in Figures 1A and B.

A dike length and thickness dataset was compiled. The length of each of the dikes selected was measured using a tape measure; only dikes with crack tips exposed at both ends were selected for measurement. The thickness of the dike was then measured at regular intervals. For the majority of the dikes, this was done by hand in the field. For a few of the largest dikes measured, this was done using scaled photographs. All measured thicknesses were then corrected for the dip angle of the dike to give the true thickness. A total of 1068 thickness measurements along the length of 41 dikes are presented; some of these are thought to be en echelon segments of a single dike; for simplicity we treat each segment individually as if they were separate dikes, referring to them as dikes rather than dike segments. We will address this simplification later on in the Discussion. The Isle of Rum dikes have a thickness:length ratio ranging from 1:11 to 1:449, with an average of 1:56. The measured lengths range between 0.08 and 47.6 m; the measured thicknesses range

between 0.007 m and 0.62 m with an average maximum thickness of 0.052 m. For most dikes the thickness measurements are accurate to about 2 mm. The largest dikes have thicknesses that are accurate to within 5 mm, and lengths that are accurate to the nearest 0.05 m. The smallest dikes are likely to be part of a segmented dike, or offshoots from a larger dike, and are not expected to have travelled far. The dikes intruded contact metamorphosed Torridonian Sandstone. Most dikes show pronounced chilled margins of at least a few millimeters (Figure 2A) and many show internal cooling fractures (Figure 2B). Many Rum dikes exhibit crack tip infilling with sediment (Figure 2A) and some show branching. Most dikes cross-cut pre-existing bedding and joints, or are themselves affected by post-emplacement jointing (Figure 2B). Few dikes have joint controlled orientations (Figure 2C) and those affected by a previous joint set were not included in the analysis. Occasional host rock inclusions are seen (Figure 2B).

The Swartruggens Kimberlite Dike Swarm

The Swartruggens Kimberlite Dike Swarm, Helam Mine, South Africa, comprises three dikes; two kimberlites (Main and Changehouse dikes) and a lamprophyre (Muil dike). The dikes intruded at the end of the Jurassic (Allsopp and Barrett, 1975; Phillips, 1991; Gurney and Kirkley 1996), and cut a stratigraphy comprising dolerite, quartzite, shale and andesite lava from the Proterozoic Pretoria Group, central Kaapvaal craton. The estimated magma emplacement depth is 2-3 km (Brown et al. 2007). Mine excavations extend to 750 m deep and give a three-dimensional view of the structure of the kimberlite dikes. A unique dataset of 683 dike-thickness measurements from Levels 16-21 of John's dike segment, and 704 dike thickness measurements from Levels 19-22 of Edward's dike segment are presented. The measurements were made by hand using a tape measure by a number of geologists systematically since the mine has been

115 active. A simplified diagram of the field relationships of these dike segments is shown in Figures
116 3A and B.
117
118 The Main dike comprises a series of anastomosing en echelon segments extending 7 km (Basson
119 and Viola 2003). The dike segments trend approximately east-west with a thickness:length ratio
120 of ~1:1000; each segment strikes approximately 1 km in length with a mean thickness of 0.64 m
121 (Kavanagh 2010; Kavanagh and Sparks, 2011). The measurements made of dike thickness are
122 accurate to the nearest 0.05 m. The lateral extent of the mined excavation is used as a proxy for
123 the breadth of the dike as this closely follows the dike geometry; the errors associated with this
124 measurement are estimated at less than 10 meters. Breccia zones up to several tens of meters
125 wide occur in the regions between dike segments, where centimeter-sized angular country rock
126 fragments have formed (Brown et al. 2007). These fragments occur as inclusions within the
127 kimberlite. Spheroidally weathered dolerite is associated with breccia zones and centimeter-thick
128 dike-parallel fracture zones that occur in the host rock at the dike margins (Brown et al. 2007).
129 The country rock away from the dike is unbrecciated, lacking closely spaced fracturing and
130 spheroidal weathering.

131 The Swartruggens dikes are not thought to be controlled by pre-existing fractures, having instead
132 created and intruded their own fractures during ascent. The host rock is jointed with no dominant
133 orientation, is brecciated especially near the fracture tips, and there is evidence for stoping
134 (Brown et al. 2007). Chilled margins were not recognized in the Swartruggens dikes; they likely
135 existed but are obscured by post-emplacement serpentenization. Closely-spaced host rock
136 fracturing, predominantly sub-parallel to the dike contact, is pervasive in the vicinity (0.1 to 1 m)
137 of the Swartruggens dike margins.

3. Theoretical framework and comparison with field data

Elasticity theory (e.g. Timoshenko and Goodier 1970, Landau and Lifshitz 1986) describes the two-dimensional shape of a fluid-filled fracture subjected to a stress field in a homogenous and isotropic material (Sneddon 1946, Pollard and Muller 1976):

$$u_y = \frac{l \sin\theta}{2G}\left[\left(P_o - S_{yo}\right)(1-v)\right] = \frac{l \sin\theta}{2G}\left[(\Delta P)(1-v)\right] \equiv A \sin\theta \quad (1)$$

$$u_y = \frac{l^2 \sin 2\theta}{16\, G}\left[\left(\nabla P - \nabla S_y\right)(1-v)\right] \equiv B \sin 2\theta \quad (2)$$

where l and u_y are the crack length and displacement, θ is the angular position along the slit from the crack centre, G is the elastic shear modulus, P_o and S_{yo} are the magma pressure and regional stress normal to the crack, ΔP is the excess magma pressure P_o - S_{yo}, v is the host rock's Poisson's ratio, ∇P is the magma pressure gradient along the crack, ∇S_y is the regional normal stress gradient along the crack, and A and B are constants. Model parameter values are given in the caption to Figure 4.

The overall displacement of the margins of the fluid filled crack is the result of a summation of both Equations (1) and (2). Equation (1) gives the displacement due to the application of a uniform internal pressure with no gradient in regional stress, whilst Equation (2) gives the displacement as a result of a linear gradient along the dike length as the difference between the regional stress and magma pressure. Models including a constant driving pressure plus a gradient in driving pressure or regional stress along the dike length will create a dike profile with a

161 teardrop shape (Pollard 1987). Asymmetrical dike profiles have been attributed to gradients in
162 magma pressure or regional stress with the magnitude of asymmetry being controlled by the
163 length of fracture, overpressure and effective stress gradient (Pollard and Muller 1976).
164
165 We analyze dike-thickness measurements from the two datasets using the method of Pollard and
166 Muller (1976). Equations (1) and (2) were iterated through 10,000 permutations of A and B to
167 estimate the best parameter values that minimize the least squares misfit between the model and
168 the observations. Overpressures and linear stress gradients are estimated from the best-fit
169 models. The estimated values of overpressure and linear stress gradient are then used as a
170 reference for comparison with the field data. These equations have been used to generate a model
171 to fit the shape of an observed solidified magma filled crack. By interpreting the static shape, the
172 assumption has been made that the fluid filled crack had reached a static equilibrium and that
173 flow effects as solidification occurred can be neglected.
174
175 **4. The shapes and thicknesses of the dikes**
176 Figure 4 shows examples of representative dike profiles for Rum and Swartruggens as horizontal
177 cross-sectional slices. It is assumed that the cross-sectional profile of the dikes at each field
178 locality is approximately horizontal. The best fitting elastic model is shown as the solid black
179 line. Overpressures estimated from the models range from 37-1990 MPa, averaging 678 MPa
180 (R^2=0.389-0.997, average=0.921) for Rum, and from 4-40 MPa (R^2=0.50-0.72) for Swartruggens
181 (Table 1). Estimated regional stress gradients for the Rum dikes estimated from the theory are up
182 to 3 GPa m^{-1}, averaging 622 MPa m^{-1}, and range from 15-87 kPa m^{-1} for Swartruggens (Table 1).

183 A comparison of the values of overpressure and stress gradient estimated for the Rum and
184 Swartruggens dikes with values obtained by previous studies are also given in Table 1.
185
186 The range of R^2 values for the best-fit models indicate that many of the dike segments do not fit
187 the elastic model well. In Figure 4 the data have been normalised (L*) to the overall length of
188 each dike giving the tips at -0.5 and +0.5. This normalization procedure allows us to compare the
189 dikes of different length scales, and to compare all the data with the elastic model in one
190 diagram.
191
192 In Figures 5A) to D), all thickness measurements have been referenced to the model fit which is
193 plotted as a horizontal line in the normalised co-ordinates to show departures in dike thickness
194 from the model. Figures 5C) and D) show the same graphs as Figures 5A) and B) but with a
195 larger scale on the y-axis. Negative y-axis values indicate a dike which is thicker than predicted
196 by the model, while positive values show a dike that is thinner than predicted. Frequency
197 histograms of the difference between the modelled thickness and the measured thickness for the
198 Rum and Swartruggens dikes are shown in Figures 5E) and F), respectively. For both localities,
199 the distribution of the data from the central portions of the dikes (L* = -0.3 to 0.3; red bars) is
200 positively offset from 0 on the x-axis whilst the distribution of the data from the edge portions of
201 the dikes (L*<-0.3 and >0.3; black bars) is negatively offset from 0 on the x-axis. The mean
202 average difference between the model and the measured data in the central portion is 0.11 for the
203 Rum data, and 0.02 for the Swartruggens data, whilst for the edges the difference is -0.10 for the
204 Rum data and -0.29 for the Swartruggens data. The Rum and Swartruggens dikes both show,

205 irrespective of goodness of fit, that dikes strongly tend to be thicker than expected by the model
206 at their edges and thinner than expected in their centers.
207
208 Our data shows dike segments are commonly asymmetrical about their length mid-point. In plan-
209 view, the Swartruggens dikes and many Rum dikes are skewed so the point of maximum
210 thickness is not at the dike centre (e.g. Figure 4B). We have quantified dike asymmetry (δ) by
211 comparing the best-fit model centre with the dike's normalized length mid-point: a δ of 0 is
212 symmetrical and 0.5 is maximum possible asymmetry. For the Rum dikes, δ ranges from 0-0.47
213 (average 0.142, standard deviation (s.d.) 0.110), for the Swartruggens dike John segment δ
214 ranges from 0.087-0.203 (average 0.154, s.d. 0.054), and from 0.179-0.242 (average 0.205, s.d.
215 0.031) for the Edward segment. The Rum dikes have a broader range of δ values; some dikes
216 show extreme asymmetry. The Swartruggens dikes are more skewed than the Rum dikes with
217 less variation in δ. We found no correlation between asymmetry and dike size. Neighbouring
218 segments commonly show asymmetry in alternating directions which may be the result of
219 compression as one dike segment influences the next one (e.g. Pollard et al. 1982, Roman and
220 Cashman 2006).
221
222 **5. Discussion**
223 We first discuss dike segmentation and our simplified analysis, before discussing the two kinds
224 of mismatch we found between the elastic theory and the observations: estimated overpressure
225 and stress gradient values are implausibly high, and dikes are systematically thicker at the edges
226 and thinner in the middle.
227

228 Segmented dikes

229 Some of the dikes measured on Rum are individual dikes (4) (Figure 6A) whilst others are
230 segments of a larger dike (37) (Figure 6B). The Swartruggens dikes are segments of a larger
231 regional intrusion. Previous workers have treated segmented dikes both as individual intrusions
232 or have modelled the segments together as one intrusion (e.g. Pollard and Muller 1976, Delaney
233 and Pollard 1981, Baer 1991 and Poland et al. 2008). Dike segmentation commonly occurs in
234 response to stress field rotation or propagation at an angle to the principal stress directions,
235 giving a series of en echelon dike fingers, or segments, with systematic step-overs between
236 segments owing to tangential stress on the dike walls (Pollard 1987). Segmentation may also
237 reflect dike propagation through heterogeneous geological media with local deviations of the
238 stress field. The Swartruggens dikes and most of the Rum dikes are better interpreted with the
239 latter explanation as the segments step direction is non-systematic. Segmentation implies a more
240 complicated local stress regime than a static elastic theory based on a fluid filled crack and these
241 complications are not easily qualified. Indeed the correct mathematical treatment of this complex
242 problem requires knowledge of the principal directions, principal stresses and magma
243 overpressure distribution along the fluid-filled crack (Meriaux and Lister, 2002); *a priori*
244 estimates based solely on dike orientations can lead to significant errors in the principal stress
245 values (Meriaux and Lister, 2002), and thus the quantification of dike segmentation.

246

247 Additionally, we note some difficulties in treating a dike with several segments as a single dike.
248 Although in some cases this can provide a better fit to the thickness data (e.g. Delaney and
249 Pollard 1981, Poland et al. 2008), especially if the thickness close to the tips is not measured, the
250 quality of the fit inherently depends on the amount of data and their position along each segment.

Our dike thickness measurements have a high frequency, including measurements made at the segment tips. As the thickness decreases to zero at the tips, this cannot be properly fit by a single opening curve for a set of segments. In addition, the true lateral extend of a segmented dike is rarely known for certain. Yet, this information is crucial as it constrains the overpressure estimate: all else being equal, a larger dike length will provide a lower overpressure estimate to explain the observed dike thickness.

A simplified static analysis whereby a segmented dike is represented by a series of collinear, identical and equally spaced segments with the same overpressure ΔP allows the opening u_s of the segments along their length $2a$ to be calculated analytically as a function of their overpressure, length and spacing (Tada et al. 2000, Gudmundsson 2011):

$$u_s = \frac{2\Delta P(1-\nu)}{\pi G} a(1+s)\left\{\ln\left[\cos\left(\frac{\pi x}{2(1+s)}\right)+\sqrt{\cos^2\left(\frac{\pi x}{2(1+s)}\right)-\cos^2\left(\frac{\pi}{2(1+s)}\right)}\right]-\ln\left[\cos\left(\frac{\pi}{2(1+s)}\right)\right]\right\}. \quad (3)$$

ν is the host-rock Poisson's ratio, G its shear modulus, and the tip-to-tip distance d between adjacent dike segments is normalised to the segment length: $s = d/2a$. Figure 7 shows how much the opening of multiple segments differs from that of a single one with the same overpressure. Closer dike segments have greater openings, but even for dike segments separated by 1/1000 of their length this opening is increased only by a factor of less than five (Figure 7B). The segment openings are proportional to their overpressure, and consequently this simplified analysis suggests that, by considering each segment separately, the overpressure is overestimated by a factor of about five. A more robust analysis would consider the relative positions of observed segments, but this would require a numerical treatment. However, the contribution of segments with larger spacing would be lower, and could offset some of the closest segments.

To investigate further the effect of analyzing dike segments collectively rather than separately, we have compared this analysis with the profile of six en echelon dikes from one locality on the Isle of Rum. The dikes at this particular locality are thought to be a completely exposed segmented dike; at all other localities where the dikes were segmented the complete extent of the dike is less certain. These six dike segments are not truly collinear, however. There is always some separation, as measured normal to one segment, and they also tend to overlap, with both separation and overlap distances varying significantly from a pair of segments to one another. We have thus used the collinear, segmented dyke analysis with a range of tip-to-tip spacing between segments, from 1 m down to 0.1 mm. As for the previous analysis, equation (3) was iterated through 1000 permutations of ΔP to estimate the best overpressure value that minimizes the least squares misfit between equation (3) and the measured opening for each segments. The best overpressure estimates range from 73 MPa to 1906 MPa with an averaged estimate of 430 MPa. The highest estimate, found for only one of the six segments, is an order of magnitude higher than the other five estimates; adjacent segments belonging to the same dike should have similar overpressures. Neglecting this highest value gives an average overpressure estimate of 135 MPa. Although these values are lower than those estimated with Pollard and Muller's analysis, the best overpressure estimates predicted by the segment analysis are still much higher than values documented in previous studies (Table 1). Figure 8 shows the best-fit profiles for both single-dyke and segmented-dyke analyses for two of the selected segments. Both analyses fail to explain the thick edges displayed by the segments (Figure 8A). Additionally, the segment analysis only deals with constant stress, and so cannot say anything about regional stress gradients nor explain the asymmetrical, teardrop shape displayed by most segments (Figure 8B).

296

297 Finally, several of the Rum segments overlap. We are not aware of any analytical solution for
298 estimating overpressures, stress gradients or shape for overlapping segments; this would require
299 numerical computations. Considering a constant overpressure, Pollard et al. (1982) showed that
300 overlapping segmented dikes would be fatter than a single one. So by considering each segment
301 as an individual dike, one would overestimate its overpressure. This overestimation will increase
302 with the number of segments that constitute a whole dike, but will decrease for increasingly
303 overlapping segments and higher rotation angle between the segment direction and that of the
304 main dyke (Pollard et al., 1982). Overlapping segments will also tend to induce segment
305 asymmetry as well as pinching or thinning of the edges (Pollard et al. 1982). This could
306 potentially explain the extremely high stress gradients derived from Pollard and Muller's analysis
307 as well as some of the pinched segment profiles. However this cannot explain the overall,
308 general shape pattern displayed by both the Rum and Swartruggens dikes: all these dikes appear
309 fatter at their edges than predicted by both Pollard and Muller's and the segmented analyses, and
310 they would appear even fatter for overlapping, pinching segments.

311

312 Considering all these limitations and effects together, it seems our single dike analysis would
313 overestimate overpressures by at most a factor 10, and appears to be the best analytical method
314 for fitting the measured profiles. Therefore, treating each segment as an individual dike provides
315 a fairer assessment of their overpressure, stress gradient and shape.

316

317 Overpressure and stress gradients

318 The elastic model of Pollard and Muller (1976) fits the data poorly for most of our studied dikes.
319 The first mismatch between the data and the elastic model is the calculated values of
320 overpressure and stress gradient which are very large. This is evident from the comparison with
321 the values estimated in previous studies (Table 1) (Geshi et al. 2010, Poland et al. 2008, Pollard
322 and Muller 1976). The overpressures are especially large and likely unphysical for the Rum
323 dikes, while the Swartruggens dikes' values are large but more plausible. The stress and
324 overpressure gradients calculated are mostly implausible for both examples. If the Rum dikes
325 with lengths < 1 m are neglected, the range of estimated overpressure values is unchanged (37 –
326 1990 MPa), although the average is slightly reduced to 398 MPa. If the Rum dikes with
327 thicknesses < 0.05 m are neglected, the estimated values of overpressure are 70 – 1990 MPa,
328 averaging 710 MPa. There appears therefore to be no dependence of these results on dike size.
329 One could reduce these overpressure and stress gradient estimates by up to an order of
330 magnitude if we consider each dyke individually and not as segments from a larger dike (see
331 previous section). Yet the majority of these estimates remain much higher than values reported in
332 previous studies (Table 1).
333
334 Very high values of overpressures and stress gradients cannot be explained using an elastic
335 model. A rock's tensile and compressive strengths are typically of order 10 MPa and 50 MPa
336 respectively, whilst magma overpressures have been estimated at <20 MPa (Stasiuk et al. 1993,
337 Gudmundsson 1999). For a 20 MPa magma source overpressure (the magma pressure in excess
338 of the regional, compressive tectonic stress), a dike propagating 1 km from its source would
339 experience a regional stress gradient of ≤20 kPa m^{-1} (Jaupart and Allegre 1991) and this stress
340 gradient estimate would decrease as the dike propagates further from its source. A dike driven by

buoyancy would have a driving stress gradient of $\Delta\rho g$, where $\Delta\rho$ is the density difference between the magma and the host rocks and g is the gravitational acceleration. A magma-host density difference of 100 kg m^{-3} gives a stress gradient of only 1 kPa m^{-1}. Stress gradients as high as those estimated for the Rum and Swartruggens dikes would therefore necessitate magma buoyancies greatly in excess of natural values governed by density differences between magmas and host rocks.

The fracture toughness of a rock is important in terms of the dike opening. According to Linear Elastic Fracture Mechanics, the intrusion of magma into a rock requires the concentration of stress at the intrusion tip to exceed the fracture toughness K_c of that rock (Pollard, 1987). This is equivalent to having an overpressure greater than $\sim K_c/(L)^{1/2}$, where L is the length of the magma-filled crack. Rocks with higher fracture toughness both require higher magma overpressure for the dikes to propagate and induce greater blunting of the dikes at their tip. Laboratory measurements of fracture toughness give values on the order of 1-10 MPa $m^{1/2}$, and so kilometer-long dikes would be expected to propagate with overpressures of 1 MPa. Larger dikes would require even lower overpressures. Conversely, our estimated overpressures would suggest rock fracture toughness of the order $10\text{-}10^4$ MPa $m^{1/2}$ and $10^2\text{-}10^3$ MPa $m^{1/2}$ for the Rum and Swartruggens dikes, respectively. These are much higher values than measured in the laboratory (e.g. Schmidt and Huddle, 1977), but similar to other field-based fracture toughness estimates (Delaney and Pollard, 1981; Delaney et al., 1986; Reches and Fink, 1988, Gudmundsson 2009). Such high values are either explained by large confining pressures at the time of dike intrusions or extensive inelastic deformation ahead and around the dike tip (Delaney et al., 1986; Rubin, 1993; Fialko and Rubin, 1997). The former explanation would necessitate depths of intrusion

364 greater than that of the Rum and Swartruggens dikes, whilst the latter explanation is plausible but
365 requires extensive inelastic deformation.
366
367 Various non-elastic explanations could be invoked to explain the high estimated overpressure
368 and stress gradient values. If the elastic parameter values used in the model were too large, the
369 overpressures and stress gradients would be overestimated. Dikes may form through the dilation
370 of pre-existing fractures that are suitably orientated with regards to principal stress directions
371 (e.g. Gudmundsson 1984, Delaney et al. 1986, Valentine and Krogh 2006), reducing the stress
372 required to fracture the host-rock. Once a fracture is re-sealed, the probability of a fracture
373 reinitiating in the same location is greater (the host-rock's *compliance*) and the shear modulus of
374 the rock can be reduced by a factor of 2 or 3 (Worthington and Lubbe 2007, Kavanagh 2010),
375 effectively making the crust less rigid. For the Rum dikes showing evidence of intruding host-
376 rocks with many pre-existing joints, the compliance may have been significant. The opening of a
377 dike is linearly proportional to its overpressure and inversely proportional to the shear modulus
378 of the host rocks (e.g. Pollard, 1987). Therefore, accounting for the compliance can only partly
379 explain the large overpressures estimated for the Rum dikes; typical changes in elastic properties
380 due to compliance would only alter the calculated values by about a factor of 3 in the Rum and
381 Swartruggens cases.
382
383 Magma extrusion from a greatly pressurised chamber into surrounding rock also provides an
384 explanation for high calculated overpressures, particularly on Rum. Magma chamber
385 overpressure increases during edifice growth until edifice destruction occurs (Pinel and Jaupart
386 2000, Pinel and Jaupart 2003, Pinel and Jaupart 2004). The Rum dikes may represent magma

extrusion from a chamber during the high-overpressure edifice-building stage. Typical stratovolcanic cones exert a load of approximately 50 MPa, significantly affecting the rock stresses beneath the volcanic edifice (Pinel and Jaupart 2003). Edifice size strongly affects the critical magma overpressure required for eruption, which may be much larger than the host-rock tensile strength (Pinel and Jaupart 2003). This is a more plausible model for explaining some of the overpressures calculated for the Rum dikes as a volcanic edifice was present at the time of diking.

High overpressures may also be partly attributed to shear failure. Assuming a shear component is present whilst diking occurs, dikes may tend to be wider than otherwise expected, leading to higher calculated overpressures. A shear component could be caused along the dike length if intrusion occurs in an orientation divergent from σ_1, as would be likely when intruding pre-existing joints. This is consistent with the offset and overlapping dike segment pattern commonly seen on Rum, suggesting propagation along non-principal stress directions.

Both Rum and Swartruggens dikes give very high calculated stress gradient values, much larger than the values estimated from previous studies (Table 1). Assuming constant elastic properties and local horizontal magma pressure, the calculated stress gradients represent mainly horizontal gradients in crustal stress. Taking a calculated stress gradient value of 65 kPa m^{-1} for a Swartuggens dike, the crustal stress normal to the dike would change by 65 MPa over a 1 km region, an implausibly large horizontal value in the upper crust. This stress gradient would require a surface topography change of about 3 km, which is unlikely in this region of southern

409 Africa. The Rum dikes give calculated stress gradients that are two orders of magnitude larger;
410 even with very strong lateral stress gradients, these values are extremely large.
411
412 A lateral variation in host rock properties has also been invoked in order to explain stress
413 gradient values (e.g. Pollard and Muller 1976, Kavanagh and Sparks 2011) as well as variations
414 in dike thickness (e.g. Baer 1991, Geshi et al. 2010). This is unlikely to be the cause of the high
415 stress gradients estimated for the Rum dikes as these intruded within one rock unit; variations in
416 burial depth along their strike would also be too small to have a significant effect.
417 Heterogeneities in the sandstone layers may add to the variations in dike thickness of the Rum
418 dikes. However, the majority have a small enough scale that even the properties of the single
419 rock unit are unlikely to have changed significantly. Variable host rock properties are thus
420 unlikely to have caused the thickness variations or the stress gradient values measured on Rum.
421
422 The cause of the dike asymmetry is most likely due to host-rock inelasticity, small scale lateral
423 host-rock property variations, and most importantly, the interference of dike edges and
424 overlapping segments. Successive emplacement of neighbouring dikes and dike segments will
425 alter the stress distribution in the host rock (e.g. Rubin and Pollard 1987). Overlapping segments
426 with solidified magma pinning the dike edges in position is the likely cause of the asymmetry
427 seen.
428
429 The dike shape
430 Changing the elastic parameters in the model does not improve the overall fit because of the
431 mismatch between the predicted and observed dike shape. The modelled dike thickness is

overestimated at the centre and mostly underestimated at the edges (Figure 5). Most of the dikes measured had a flatter central section than predicted. An active dike's width is determined by the overpressure which usually declines with time as the chamber pressure decreases, manifest by waning flow rate in many lava eruptions (Stasiuk et al. 1993), although the thickness can also be determined by the dike length for a fixed overpressure. If a dike erupts, this dike and the overall, not-yet-solidified, intrusive system will experience a reduction in overpressure. However, the majority of dikes are not thought to erupt (e.g. Gudmundsson 1984, Gudmundsson et al. 1999). Arrested dikes can still however experience a reduction in overpressure during intrusion. At neither of the studied field localities were we able to find unequivocal field evidence of the magma transport direction; these may therefore have propagated vertically or laterally. For a constant magma volume, provided that the crack is not buoyancy driven, the overpressure in an intruding crack will decrease as the length of the crack increases (Mcleod and Tait 1999). Moreover, however the intrusion is driven, its overpressure will decrease because of the viscous pressure drop it will experience during propagation (Lister and Kerr, 1991). We do not see direct evidence that the dikes from either locality connected to their palaeosurface, and therefore we must rely on indirect evidence to assess whether or not these dikes were feeders. If it can be assumed that at tens of meters depth a dike with a maximum thickness greater than one meter has the potential to act as a feeder dike (Geshi et al. 2010), the Swartruggens dike segments (which have a maximum thickness of 1.95 meters; Kavanagh and Sparks, 2011) could potentially have acted as feeder dikes. As the mean thickness of the dikes measured at both field locations is less than one meter, it is assumed that our analysis can only be applied to dikes fulfilling this criterion, and the application of our results to thicker dikes will require further investigation.

455 As magma flows through a fracture (Figure 9A), chilling of the magma at the dike margins
456 prevents it from closing at the tips (Figure 9B). Viscosity increase by preferential cooling at the
457 dike edges adds to this effect. As the overpressure wanes, if the position of the edges becomes
458 fixed and the dike is no longer propagating in the direction of the tip, the preserved thickness is
459 then determined by the initial overpressure (Figure 9C). However, the non-solid and less viscous
460 central parts of the dike can close as the overpressure declines; the initial dike injection shape is
461 not the shape that is ultimately preserved as the solidified dike. We suggest therefore that the
462 shape mismatch is principally a result of chilling and solidification during dike emplacement.
463
464 Inelasticity can also account for some of the dike thickness variation. There is strong evidence
465 for inelastic deformation in the zones between the Swartruggens dike segments, which may have
466 reduced the host-rock rigidity and shear strength. Mechanical processes such as brecciation,
467 stoping and weathering (preferentially focused at dike termination points, over-laps and relay
468 zones) can weaken the rocks prior to magma emplacement and produce an inelastic host-rock
469 response during emplacement (Brown et al. 2007, Kavanagh 2010, Kavanagh and Sparks, 2011).
470 Similar inelastic deformation between adjacent segments has been observed by Schofield et al.
471 (2010) at the Golden Valley Sill, South Africa. Additionally, small segments such as those
472 observed on Rum are likely to correspond to segments lying close to the very tip of their main
473 dike, and so to be embedded within the inelastic, damaged region that surrounds that main dyke
474 tip. Indeed, the size of this damage region tends to scale with that of the dyke that created it
475 (Faulkner et al., 2011), and could reach several meters or tens of meters (e.g. Delaney et al.,
476 1986). Inelastic deformation within the damage zone would contribute to blunting the edges of
477 the segments embedded there. Thus inelastic deformation could both explain the apparent high

478 values of rock fracture toughness, suggested by our high overpressure estimates, and the
479 observations of dike tips that are thicker than expected from elastic theory. Inelastic deformation
480 in the steps between segments also provides an explanation for those dikes which are markedly
481 asymmetric. Much more inelastic deformation at one end of the dike than the other will mean a
482 distortion of the shape that results in asymmetry. The observation of alternations in the sense of
483 asymmetry of segments indicates too that complex inelastic deformation in the step-over regions
484 has occurred.
485
486 Implications for eruption longevity and crustal strain
487 The tendency for thick dike tips and narrow centers has broader implications. The wedging of the
488 dike edges formed at high magma overpressures is made permanent by chilling. Thus as the
489 pressure reduces and the eruption wanes, the fracture will be prevented from closing fully and
490 the dike can continue to act as an open conduit for longer than it otherwise would have been able
491 to. Dike emplacement can be regarded as the accommodation of crustal strain as a response to
492 tectonic stresses. However, the dimensions of an active dike with magma pressures exceeding
493 tectonic stresses indicate that the transient strain can exceed the tectonic strain expected. Since
494 the now chilled edges have previously been pushed apart under a high magma overpressure, the
495 additional strain can be permanently preserved due to the chilled and wedged dike edges. For
496 large dikes with prolonged flow at overpressures exceeding tectonic stresses and with substantial
497 solidification along the dike edges the excess strain could be substantial.
498
499 **7. Conclusions**

Many of the dikes measured on Rum and at Helam Mine are poorly fit by the classical elastic model of Pollard and Muller (1976). There are two distinct mismatches between the presented data and the elastic model. Firstly, many dike shapes are too thin in the middle and too thick at the edges to be fit by an elastic profile; the calculated R^2 values range from 0.389-0.997 and the misfits are larger than measurement uncertainties. Secondly, even for dikes where the model fit is acceptable, the calculated magma driving pressures and linear stress gradients are very large, particularly for the small-scale basaltic dikes on Rum. Many explanations have been provided to account for the differences. Of these, the cooling of the dike edges wedging the fracture open, and the host-rock inelastic deformation pre- and syn- magma emplacement provide the most complete explanation for the mismatches between the data and the model. Care should be taken when extrapolating the observations from the dikes measured from the Swartruggens swarm and on Rum. As the mean observed dike thickness was less than a meter, it is not automatic to assume that the analysis will apply to larger dikes; the application of the results to thicker dikes will require further investigation.

Acknowledgements

KAD would like to thank R. C. Ogilvie-Harris for assistance with the Rum data collection. A. Gudmundsson, A. E. L. Ferrari and an anonymous reviewer are gratefully acknowledged for providing valuable comments to improve the manuscript. M. Poland and two anonymous reviewers are thanked for helpful comments on an earlier shorter form of the manuscript. J. Davidson and A. Rogers are thanked for permission to publish the dataset from Helam Mine. RSJS, JLK and TM were supported by a grant from the Leverhulme Trust. RSJS is co-supported

522 by an advanced grant from the European Research Council. KAD was supported by a NERC
523 Consortium Grant.
524
525

References

Allsopp, H.L. & Barrett, D.R. 1975. Rb–Sr age determinations on South African kimberlite pipes. Physics and Chemistry of the Earth, 9, 605–617.

Baer, G., 1991. Mechanisms of dike propagation in layered rocks and in massive, porous sedimentary rocks. Journal of Geophysical Research 96, 11911-11929.

Basson, I. J., and Viola, G., 2003. Structural overview of selected Group II kimberlite dyke arrays in South Africa: implications for kimberlite emplacement mechanisms. South African Journal of Geology 106 (4), 375 - 394.

Brown, R. J., Kavanagh, J. L., Sparks, R. S. J., Tait, M., and Field, M., 2007. Mechanically disrupted and chemically weakened zones in segmented dike systems cause vent localization: Evidence from kimberlite volcanic systems. Geology 35 (9), 815 - 818.

Buck, W. R., Einarsson, P., and Brandsdottir, B., 2006, Tectonic stress and magma chamber size as controls on dike propagation: constraints from the 1975-1984 Krafla rifting episode: Journal of Geophysical Research, v. 111, doi:10.1029/2005JB003879.

Delaney, P. T., and Pollard, D. D., 1981. Deformation of host rocks and flow of magma during growth of Minette dikes and breccias-bearing intrusions near Ship Rock, New Mexico. U. S. Geological Survey professional paper 1202.

Delaney, P. T., Pollard, D. D., Ziony, J. I., and McKee, E. H., 1986. Field relations between dykes and joints' emplacement processes and paleostress analysis. Journal of Geophysical Research 91 (B5), 4920 - 4938.

Domenico, S. N., 1983. Sandstone and limestone porosity determination from shear and compressional wave velocity. Bulletin of the Australian Society of Exploration Geophysicists 14 (4), 81 - 90.

549 Emeleus, C. H., 1997. Geology of Rum and the adjacent islands. British Geological Survey
550 Memoir for 1:50 000 Geological Sheet 60 (Scotland). The Stationery Office.
551 Faulkner, D. R., Mitchell, T. M., Jensen, E., and Cembrano, J., 2011. Scaling of fault damage
552 zones with displacement and the implications for fault growth processes. Journal of Geophysical
553 Research 116, B05403, doi:10.1029/2010JB007788.
554 Fialko, Y. A., and Rubin, A. M., 1997. Numerical simulation of high-pressure rock tensile
555 fracture experiments: evidence of an increase in fracture energy with pressure? Journal of
556 Geophysical Research 102 (B3), 5231 – 5242.
557 Geshi, N., Kusumoto, S., and Gudmundsson, A., 2010. Geometric difference between non-feeder
558 and feeder dikes. Geology 38 (3), 195-198.
559 Gudmundsson, A., 1983. Form and dimensions of dykes in Eastern Iceland. Tectonophysics 95,
560 295 – 307.
561 Gudmundsson, A., 1984. Formation of Dykes, Feeder-dykes, and the Intrusion of Dykes from
562 Magma Chambers. Bulletin of Volcanology 47 (3), 537 - 550.
563 Gudmundsson, A., 1999. Fluid overpressure and stress drop in fault zones. Geophysical Research
564 Letters 26 (1), 115 – 118.
565 Gudmundsson, A., 2009. Toughness and failure of volcanic edifices. Tectonophysics 471, 27 –
566 35.
567 Gudmundsson, A., 2011. Rock Fractures in Geological Processes. Cambridge University Press,
568 pp.592.
569 Gudmundsson, A. Marinoni, L. B., and Marti, J., 1999, Injection and arrest if dykes: Implications
570 for volcanic hazards. Journal of Volcanology Geothermal Research 88, 1 - 13.

571 Gurney, J. J., and Kirkley, M. B., 1996. Kimberlite dyke mining in South Africa. Africa
572 Geoscience Review 3, 191 - 201.
573 Hamilton, M. A., Pearson, D. G., Thompson, R. N., Kelley, S. P., and Emeleus, C. H., 1998.
574 Rapid eruption of Skye lavas inferred from precise UPb and ArAr dating of the Rum and Cuillin
575 plutonic complexes. Nature 394, 260 - 263.
576 Jaupart, C., and Allègre, C. J., 1991. Gas content, eruption rate and instabilities of eruption
577 regime in silicic volcanoes. Earth and Planetary Science Letters 102, 413 - 429.
578 Kavanagh, J., 2010. Ascent and emplacement of kimberlite magmas, PhD Thesis, University of
579 Bristol.
580 Kavanagh J., and Sparks, R. S. J., 2011. Insights of dyke emplacement mechanics from detailed
581 3D dyke thickness datasets. Journal of the Geological Society of London 168, 965 – 978.
582 Kerr, R. C., and Lister, J. R., 1995. The lateral intrusion of silicic magmas into unconsolidated
583 sediments: the Tennant Creek prophyry revisited. Australian Journal of Earth Sciences 42, 223 -
584 224.
585 Khazanehdari, J., and Sothcott, J., 2003. Variation in dynamic elastic shear modulus of sandstone
586 upon fluid saturation and substitution. Geophysics 68 (2), 472 - 481.
587 Landau, L. D., and Lifshitz, E. M., 1986. Theory of Elasticity, 3rd edition. Butterworth
588 Heinemann, Oxford, England.
589 Lister, J. R., and Kerr, R. C., 1991. Steady solutions for feeder dykes in a density-stratified
590 lithosphere. Journal of Geophysical Research 96, (B6), 10049 - 10077.
591 McLeod, P., and Tait, S., 1999. The growth of dykes from magma chambers. Journal of
592 Volcanology and Geothermal Research 92, 231–245

593 Menand, T., Daniels, K. A., and Benghiat, P., 2010. Dyke propagation and sill formation in a
594 compressive tectonic environment. Journal Geophysical Research 115 (B08201).
595 Menand, T., and Tait, S. R., 2002. The propagation of a buoyant liquid-filled fissure from a
596 source under constant pressure: An experimental approach. Journal of Geophysical Research 107
597 (B11), 2306.
598 Menand, T., and Tait, S. R., 2001. A phenomenological model for precursor volcanic eruptions.
599 Nature 411, 678-680.
600 Meriaux. C., and Lister, J. R., 2002. Calculation of dike trajectories from volcanic centres.
601 Journal of Geophysical Research 107 (B4), 2077.
602 Nicoll, G. R., Holness, M. B., Troll, V. R., Donaldson, C. H., Holohan, E. P., Emeleus, C. H.,
603 and Chew, D., 2009. Early mafic magmatism and crustal anatexis on the Isle of Rum: evidence
604 from the Am M`am intrusion breccia. Geological Magazine 146 (3), 368–381.
605 Phillips, D. 1991. Argon isotope and halogen chemistry of phlogopite from South African
606 kimberlites: a combined step-heating, laser probe, electron microprobe and TEM study. Chemical
607 Geology: Isotope Geoscience Section, 87, 71–98.
608 Pinel, V., and Jaupart, C., 2000. The effect of edifice load on magma ascent beneath a volcano.
609 Philosophical Transactions of the Royal Society of London A 358, 1515 - 1532.
610 Pinel, V., and Jaupart, C., 2003. Magma chamber behaviour beneath a volcanic edifice. Journal
611 of Geophysical Research 108 (B2), 2072.
612 Pinel, V., and Jaupart, C., 2004. Magma storage and horizontal dyke injection beneath a volcanic
613 edifice. Earth and Planetary Science Letters 221, 245 - 262.

614 Poland, M., Moats, W. P., and Fink, J. H., 2008. A model for radial dike emplacement in
615 composite cones based on observations from Summer Coon volcano, Colorado, USA. Bulletin of
616 Volcanology 70, 861-875.
617 Pollard, D. D., 1987. Elementary fracture mechanics applied to the structural interpretation of
618 dykes; in Mafic dyke swarms, Editors: Halls, H. C., and Fahrig, W. F., Geological Association of
619 Canada Special Paper 34, 5-24.
620 Pollard, D. D., and Muller, O. H., 1976. The effect of gradients in regional stress and magma
621 pressure on the form of sheet intrusions in cross section. Journal of Geophysical Research 81, (5),
622 975 - 984.
623 Pollard, D. D., Segall, P. and Delaney, P. T., 1982. Formation and interpretation of dilatant
624 echelon cracks. Geological Society of America Bulletin, 93, 1291-1303.
625 Ray, R. Hetu, C. S., and Jyotirmoy, M., 2007. Structure and emplacement of the Nandurbar–
626 Dhule mafic dyke swarm, Deccan Traps, and the tectonomagmatic evolution of flood basalts.
627 Bulletin of Volcanology 69, 537 – 551.
628 Reches, Z., and Fink, J., 1988. The mechanism of intrusion of the Inyo Dike, Long Valley
629 Caldera, California. Journal of Geophysical Research 93 (B5), 4321 – 4334.
630 Roman, D. C., and Cashman, K. V., 2006. The origin of volcano-tectonic earthquake swarms.
631 Geology 34 (6), 457 - 460.
632 Rubin, A. M., 1993. Tensile fracture of rocks at high confining pressure: Implications for dike
633 propagation. Journal of Geophysical Research 98 (B9), 15,919 – 15,935.
634 Rubin, A. M., 1995. Propagation of magma-filled cracks. Annual Reviews in Earth and Planetary
635 Science 23, 287 - 336.

636 Rubin, A. M., and Pollard, D. D., 1987. Origins of blade-like dikes in volcanic rift zones, in:
637 Decker, R. W., Wright, T. L., and Stauffer, P. H., eds., Volcanism in Hawaii. U.S. Geological
638 Survey professional paper 1350, 1449-1470.
639 Tada, H., Paris, P. C., and Irwin, G. R., 2000. The Stress Analysis of Cracks Handbook, 3rd ed.,
640 New York : ASME Press.
641 Timoshenko, S. P., and Goodier, J. N., 1970. Theory of elasticity. McGraw-Hill, 3rd edition, pp.1-
642 567.
643 Schmidt, R.A. and Huddle, C.W., 1977. Effect of confining pressure on fracture toughness of
644 Indiana limestone. International Journal of Rock Mechanics & Mining Sciences Geomechanics
645 Abstracts 14, 289 - 293.
646 Schofield, N., Stevenson, C., and Reston, T., 2010. Magma fingers and host rock fluidization in
647 the emplacement of sills. Geology 38, 63 - 66.
648 Sneddon, I. N., 1946. The distribution of stress in the neighborhood of a crack in an elastic solid.
649 Proceedings of the Royal Society of London A 187, 229 - 260.
650 Stasiuk, M. V., Jaupart, C., and Sparks, R. S. J., 1993. Influence of cooling on lava-flow
651 dynamics. Geology 21 (4), 335 - 338.
652 Valentine, G. A., and Krogh, K. E. C., 2006. Emplacement of shallow dikes and sills beneath a
653 small basaltic volcanic center: The role of pre-existing structure (Paiute Ridge, southern Nevada,
654 USA). Earth and Planetary Science Letters 246, 217 - 230.
655 White, R.S., Drew, J., Martens, H.R., Key, J., Soosalu, H. and Jakobsdóttir, S.S, 2011.
656 Dynamics of dyke intrusion in the mid-crust of Iceland. Earth and Planetary Science Letters
657 304, 300 - 312.

658 Worthington, M. H., and Lubbe, R., 2007. The scaling of fracture compliance. Geological
659 Society, London, Special Publications 270, 73 – 82.

660

661 **Table caption:**

662 Table 1: Estimated values for driving pressure ($P_o - S_{yo}$) and stress gradient ($\nabla P - \nabla Sy$) for Rum
663 and Swartruggens dikes (this study), non-feeder dikes at Miyakejima volcano (Geshi et al. 2010),
664 silicic dikes at Summer Coon volcano (Poland et al. 2008) and Walsen Dike and Theatre Canyon
665 Sill (Pollard and Muller 1976).

666

667 **Figure captions**

668 Figure 1: The locations of the measured dikes. A generalised geological map of the isle of Rum
669 with each of the dike measurement localities highlighted.

670

671 Figure 2: Photographs and sketches of Rum dikes. A) Plan-view of dike with crack tips showing
672 pronounced chilled margins. One crack tip shows infilling with sediment. There is overlap
673 between dike segments, one segment shows an apparent skew. B) Dike orientation unaffected by
674 secondary jointing. C) Joint affected dike orientation.

675

676 Figure 3: A) Surface outcrop map of the John and Edward kimberlite dike segments, Helam
677 Mine, South Africa. B) Contour plot of dike thickness for the John and Edward dike segments
678 plotted against depth below the current surface and distance easting. The shaded area indicates
679 locations where data has been collected. The approximate stratigraphy and unit contacts (dashed

680 line) are shown, comprising quartzite (Qtz), shale (Sh) and dolerite (Dol). The map inset
681 indicates the location of Helam Mine in southern Africa (lat -25.594º, lon 26.659º).
682
683 Figure 4: Thickness versus length profile of Rum (Figures 3A, C and D) and Swartruggens
684 (John's dike segment, 18th Level) (Figure 3B) dikes. A best-fit model (line) is plotted through
685 the data (diamonds). Both datasets show asymmetrical dike-thicknesses, with fatter edges and
686 thinner middles compared to the elastic model. Best-fit model parameter values are: A), C) and
687 D) G = 15.4 GPa (Khazanehdari and Sothcott, 2003), ν = 0.215 (Domenico, 1983), ΔP = 367
688 MPa, and ∇P = 48 MPa m^{-1}. B) G = 40 GPa, ΔP = 34 MPa and ∇P = 65 kPa m^{-1}. L* is the along-
689 dike distance normalised by the dike length and T* is the half-thickness normalised by the dike
690 length.
691
692 Figure 5: A) to D) T is dike thickness. The line at y=0 is a perfect model fit to the data. Negative
693 y-axis values indicate a dike that is fatter than the model, positive y-axis values show a thinner
694 dike than the model. Positive values are in the downwards direction. Both A) and C) the Rum
695 dikes and B) and D) the Swartruggens dikes (John segment, Levels 16-21, and Edward segment
696 Levels 19-22) have fatter edges and thinner centres than is expected from the model fit. Figure
697 4C) and D) as 4A) and B), but with the vertical axis changed to show the range of -2 to 2 in order
698 to more clearly see the distribution of the points above and below the perfect model fit (red) line.
699 It can be seen that for both field localities, the majority of the points in the central region (L* = -
700 0.3 to 0.3) show thicknesses which are narrower than expected, and at the edges (L*<-0.3 and
701 >0.3) the thicknesses are larger than expected. Frequency histograms of the difference between
702 the modelled T and the measured T for E) the Rum and F) Swartruggens dikes showing the

703 distribution of data relative to 0 (the perfect model fit) for the central region of each dike (red)
704 and the edges of each dike (black).
705
706 Figure 6: A and B) The relationship between dike tips of segmented and non-segmented dikes.
707 A) The tip of a dike with no neighboring dikes or dike segments (Rum). B) The overlapping dike
708 tips of two segmented dikes observed at locality 5 on Rum. The dike tips are separated at this
709 locality by approximately 10 cm.
710
711 Figure 7: A) Schematic diagram of a segmented dike. All the segments are identical, collinear,
712 equally spaced, and loaded with the same overpressure. Two segments are represented here, but
713 the analysis considers an infinite number of segments. B) Along-strike opening of the dike
714 segments. The along-strike position x, measured from the segment center, is normalized to the
715 segment half-length a, and the segment opening u_s to the maximum opening, $\Delta P(1-\nu)a/G$, of a
716 single dike with the same half-length and overpressure ΔP. The tip-to-tip distance d between
717 adjacent dike segments is normalized to the length of the segments: $s = d/2a$. Only half of the
718 segment length is shown ($0< L^* <0.5$). The continuous curve corresponds to the case of a single
719 dike, and the dashed curves to different normalized spacings s.
720
721 Figure 8: Opening profiles of two segments belonging to the same dike from the Isle of Rum
722 (diamonds) compared with the segmented analysis (equation 3; black curve) and the analysis of
723 Pollard and Muller (1976; dashed curve). A) Best overpressure estimates: 110 MPa (black curve)
724 and 332 MPa (dashed curve). There is no stress gradient. B) Best overpressure estimates: 73
725 MPa (black curve) and 150 MPa (dashed curve). The segmented analysis cannot explain the

726 teardrop shape of this segment. Best stress gradient estimated from Pollard and Muller's analysis
727 (dashed curve): 136 MPa/m.
728
729 Figure 9: Schematic illustration of the impact of cooling on preserved dike geometry, presented
730 as three time steps in the evolution of a horizontal section through the dike. A) Magma intrudes
731 a fracture, and B) cooling ensues at the dike margins. C) Chilled fracture tip magma props the
732 fracture open as the overpressure reduces, preventing crack closure and creating the observed
733 dike profile (solid line) with a thinner center and thicker tips. The dashed line in C) indicates the
734 expected profile of a pressurized magma-filled fracture in an elastic media.
735

Table1_Daniels

Intrusive Body	*Number of observations*	$P_o - S_{yo}$ *(MPa)*
Rum dikes	784	37 – 1990
Swartruggens dikes	1387	4 – 40
Miyakejima volcano	>88	7 – 12
Summer Coon volcano	238	4.6 – 148.3
Walsen Dike	256	0.35 – 4.8
Theatre Canyon Sill	44	3.6 – 50

$\nabla P - \nabla S_y$ (kPa m^{-1})
0 – 3 x 10^6
15 – 87
0.003 – 0.133
-0.052 – -0.71
-8.4 – -12

Figure1_Daniels

Click here to download Figure: FIGURE1_Daniels.pdf

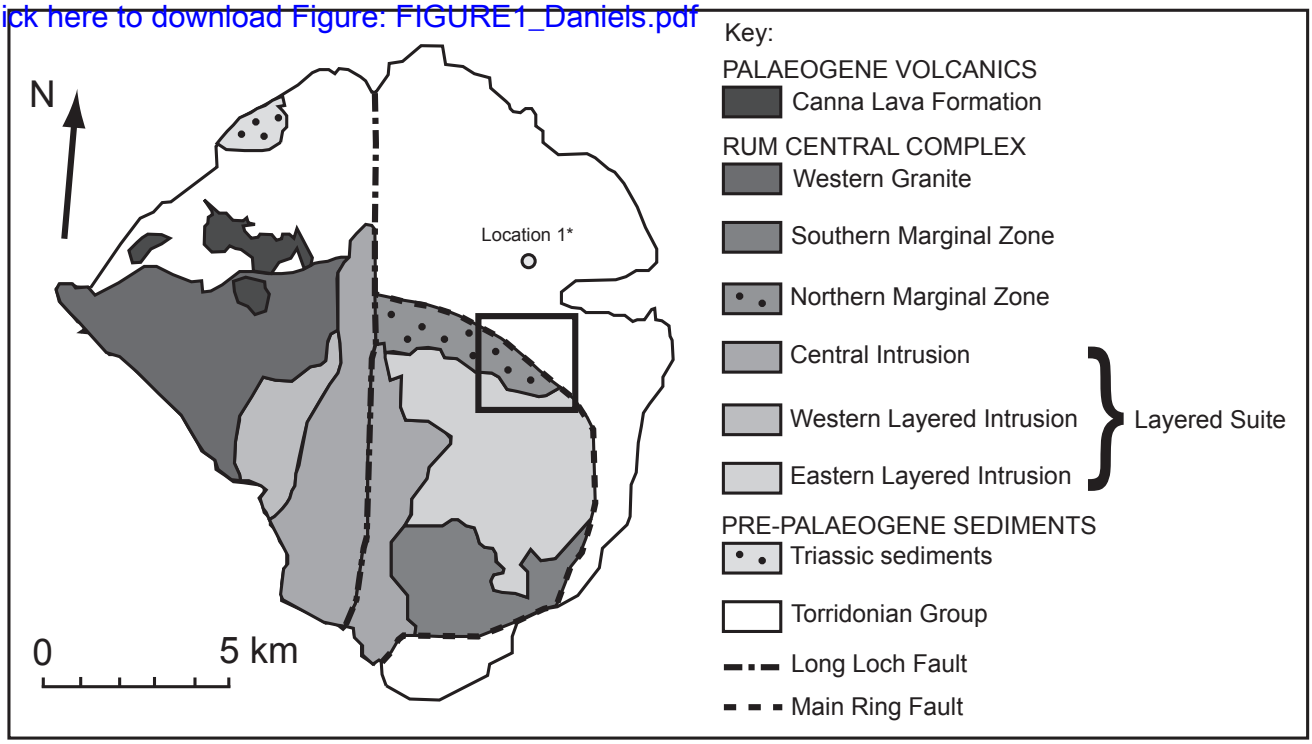

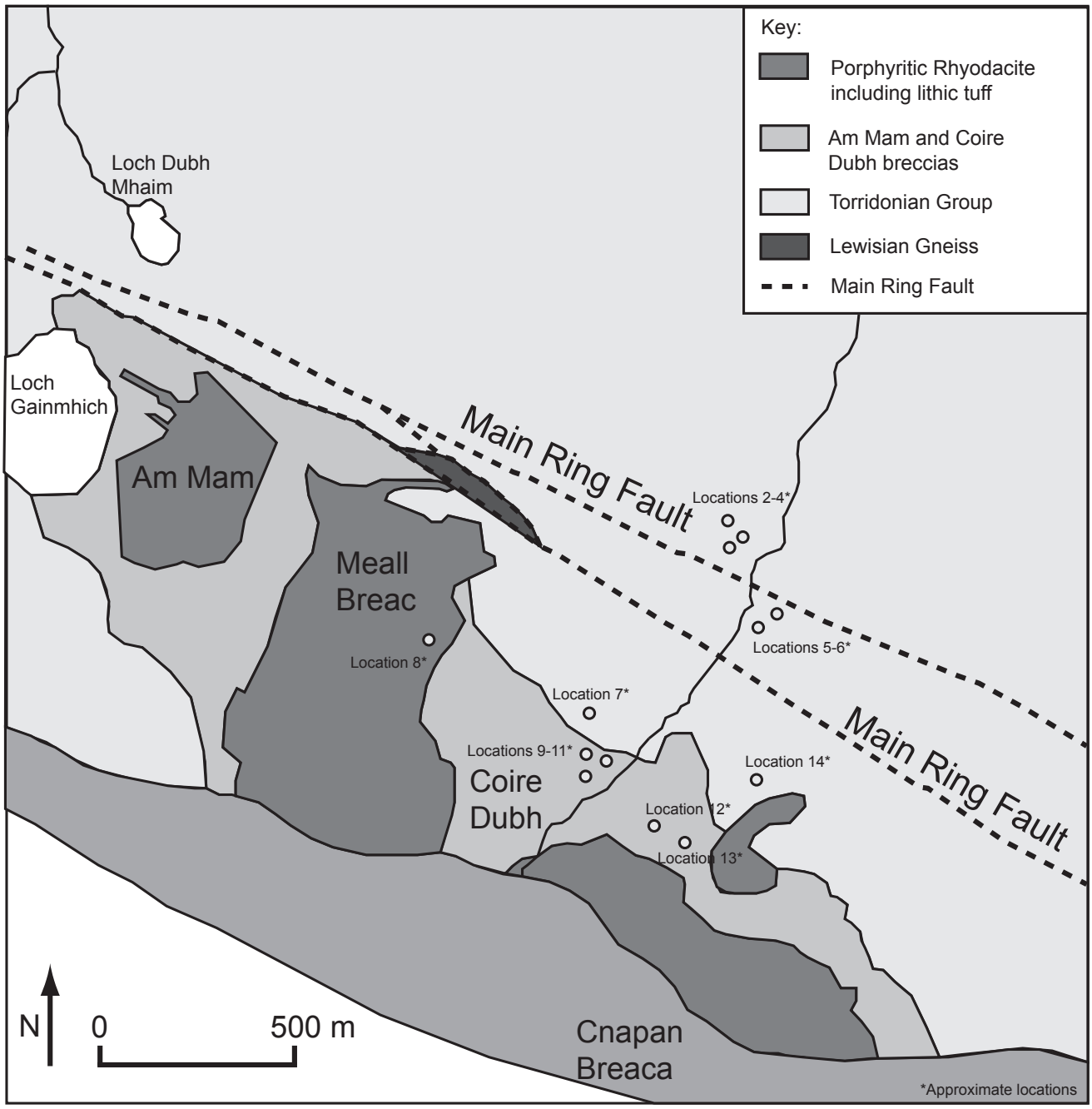

Figure2_Daniels

Click here to download Figure: FIGURE2_Daniels.pdf

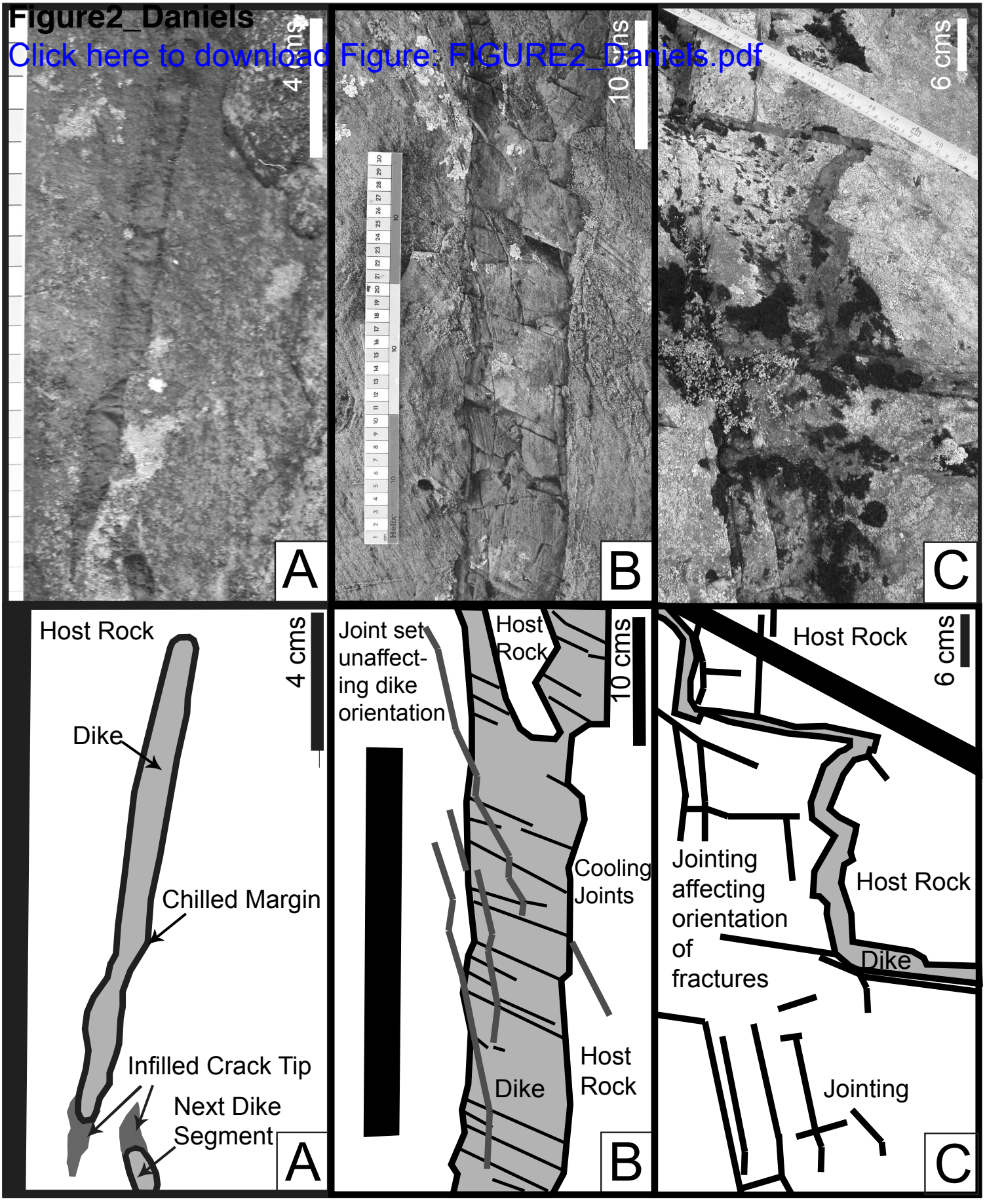

Figure3_Daniels

Click here to download Figure: FIGURE3_Daniels.pdf

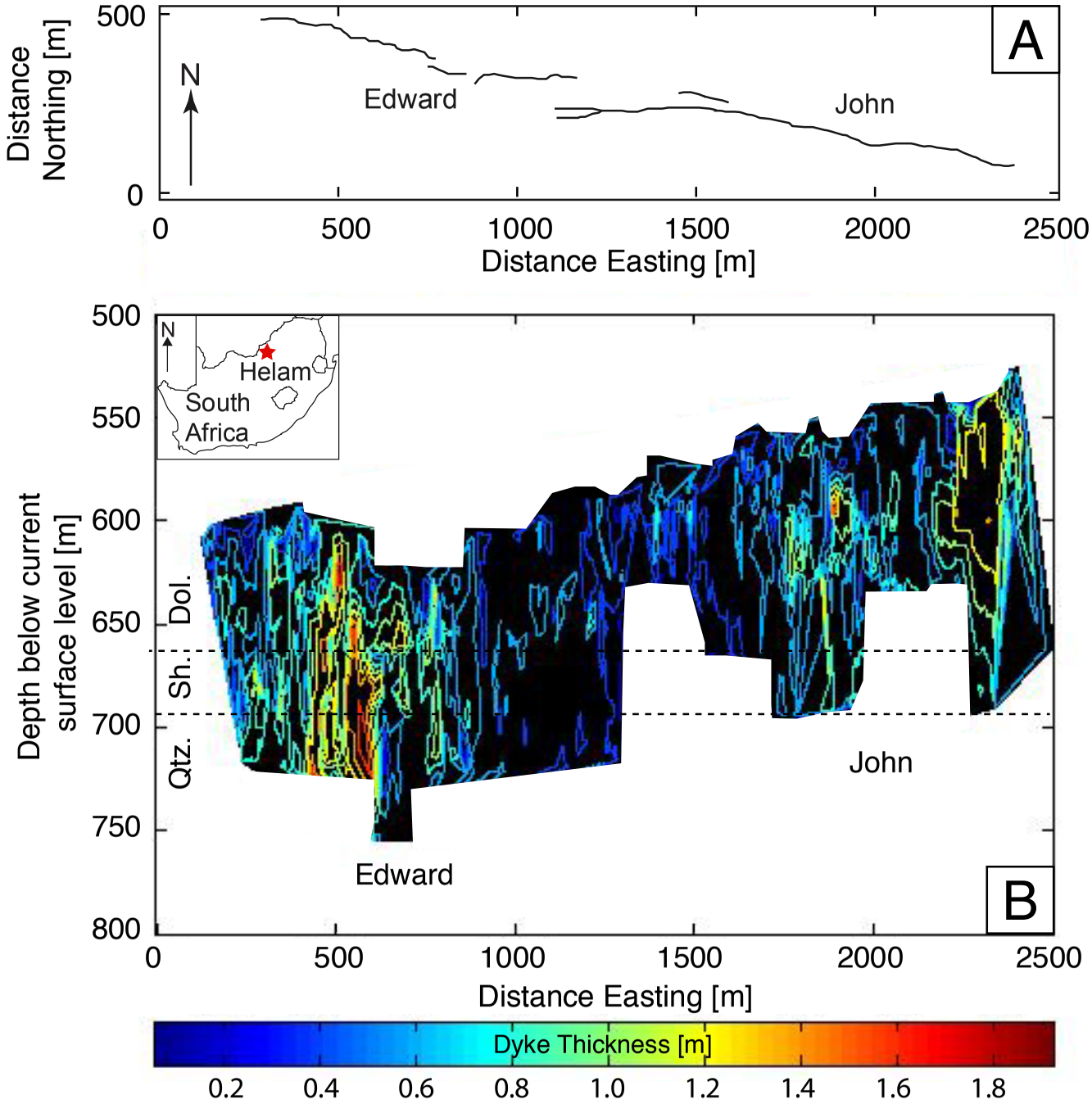

Figure4_Daniels

Click here to download Figure: FIGURE4_Daniels.pdf

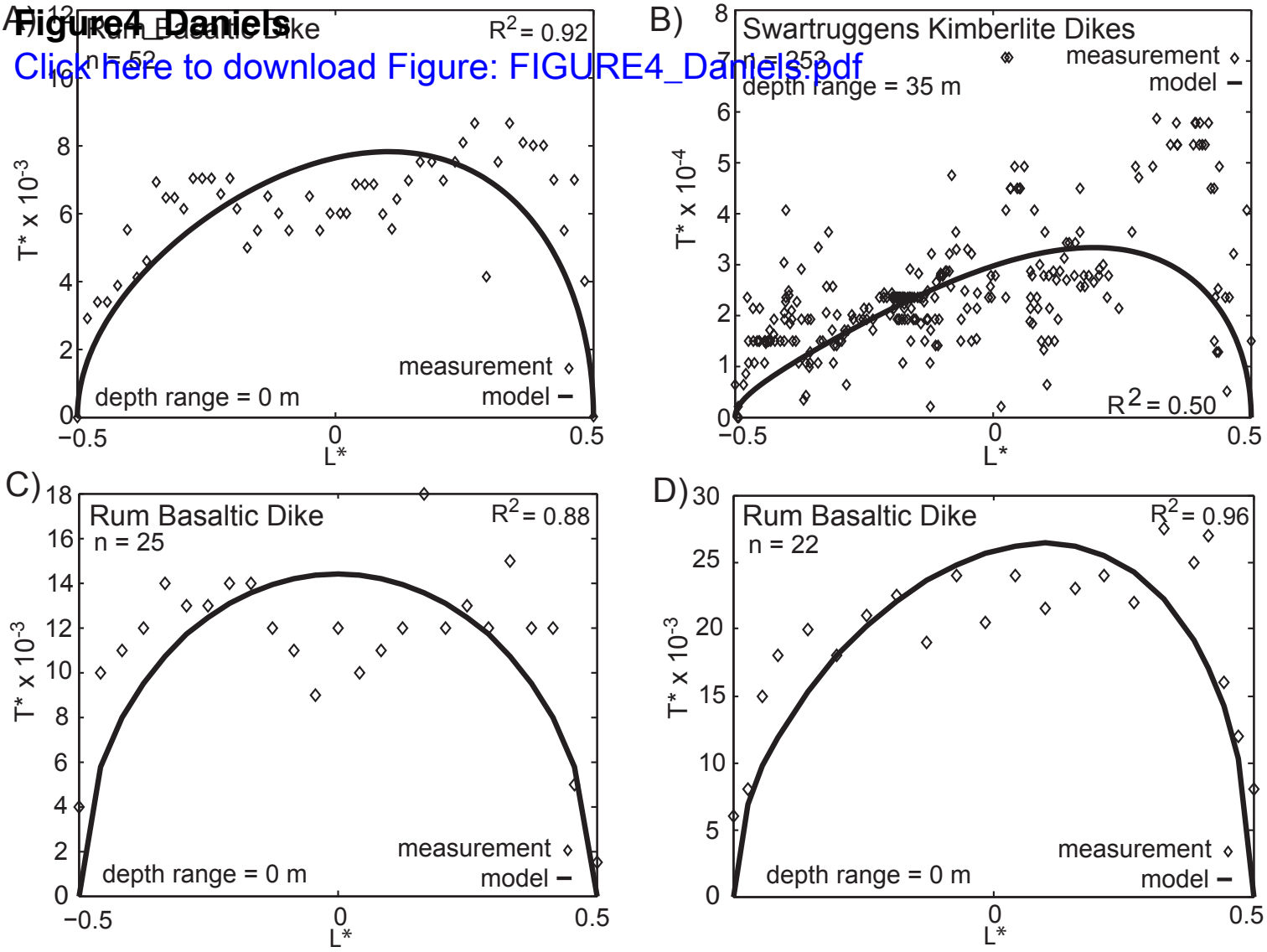

Figure5_Daniels

Click here to download Figure: FIGURE5_Daniels.pdf

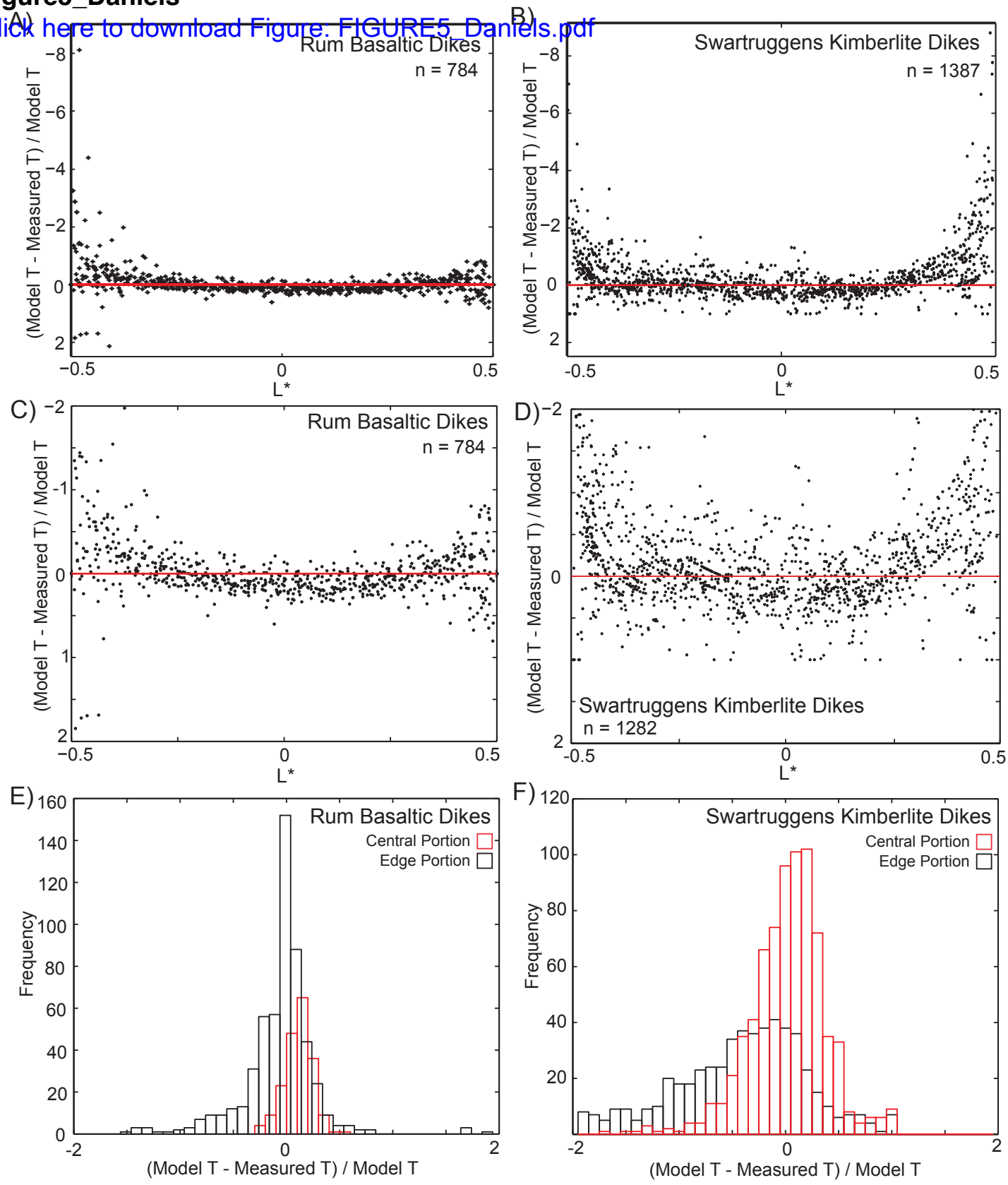

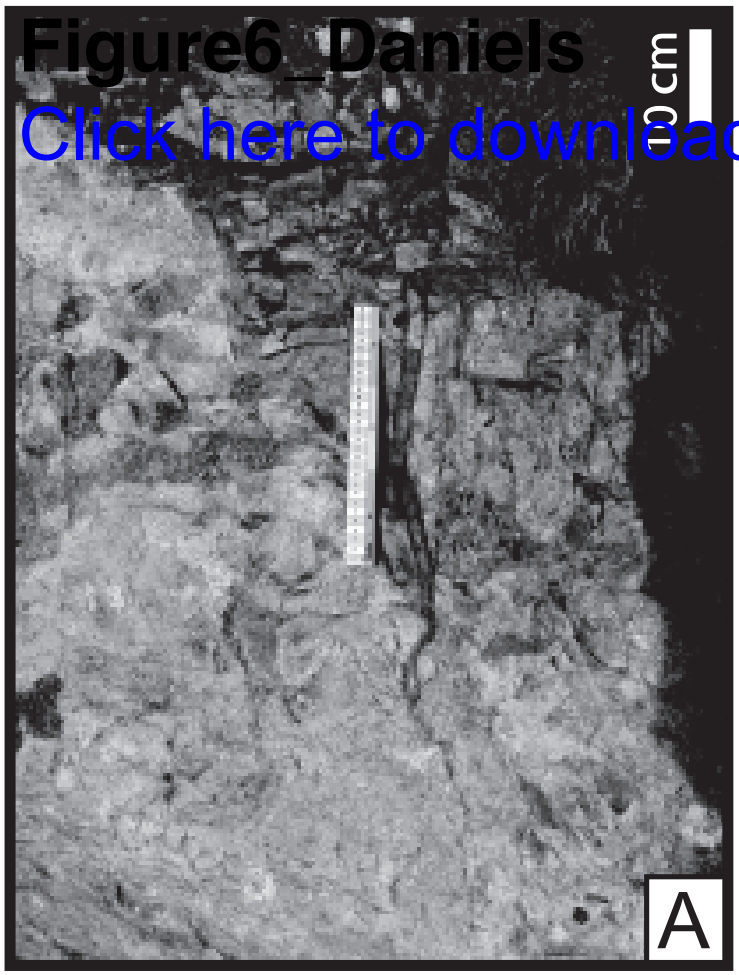

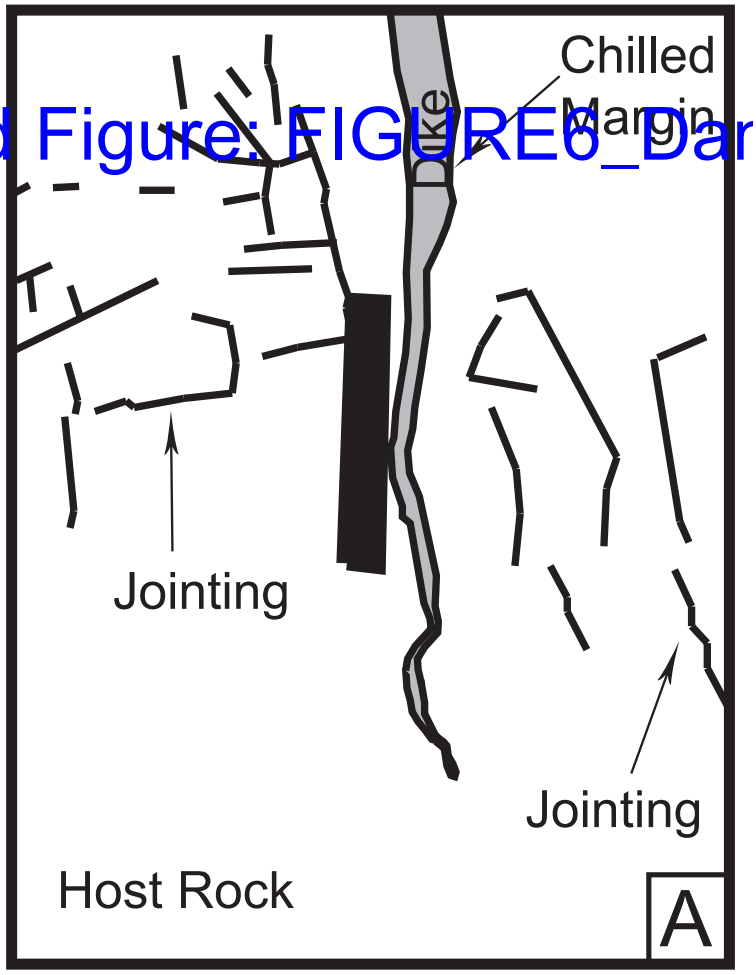

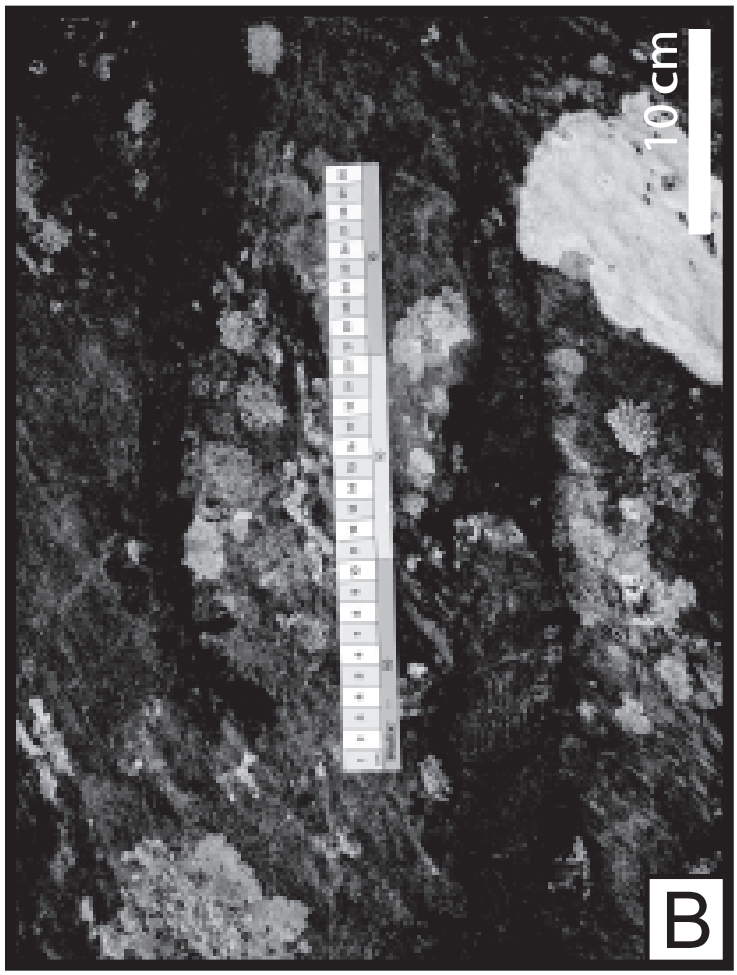

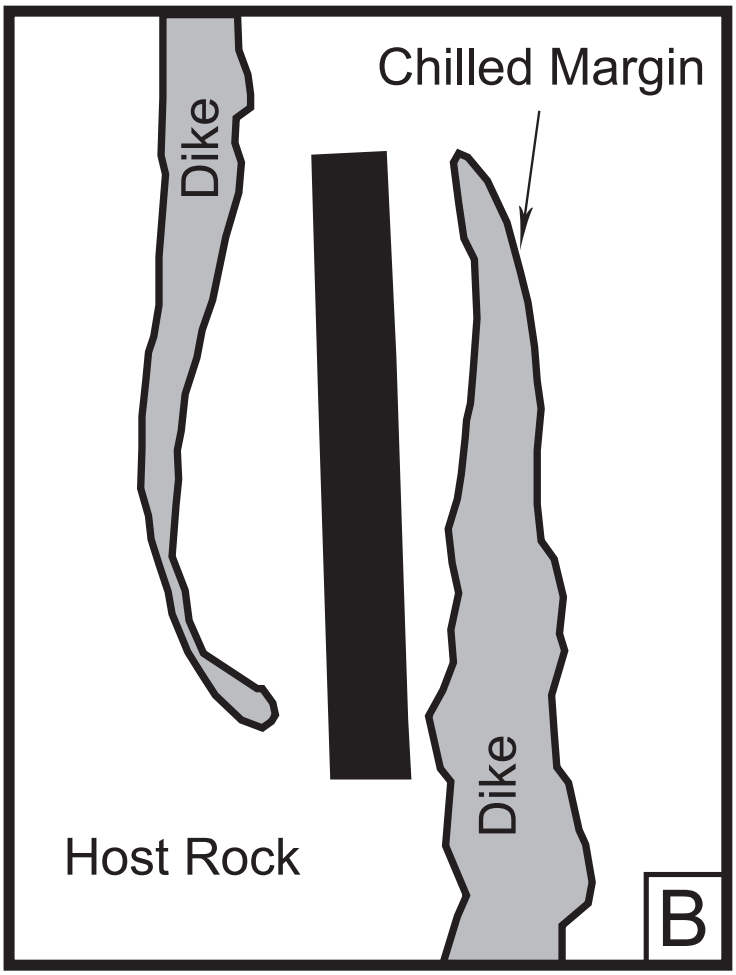

Figure7_Daniels
Click here to download Figure: FIGURE7_Daniels.pdf

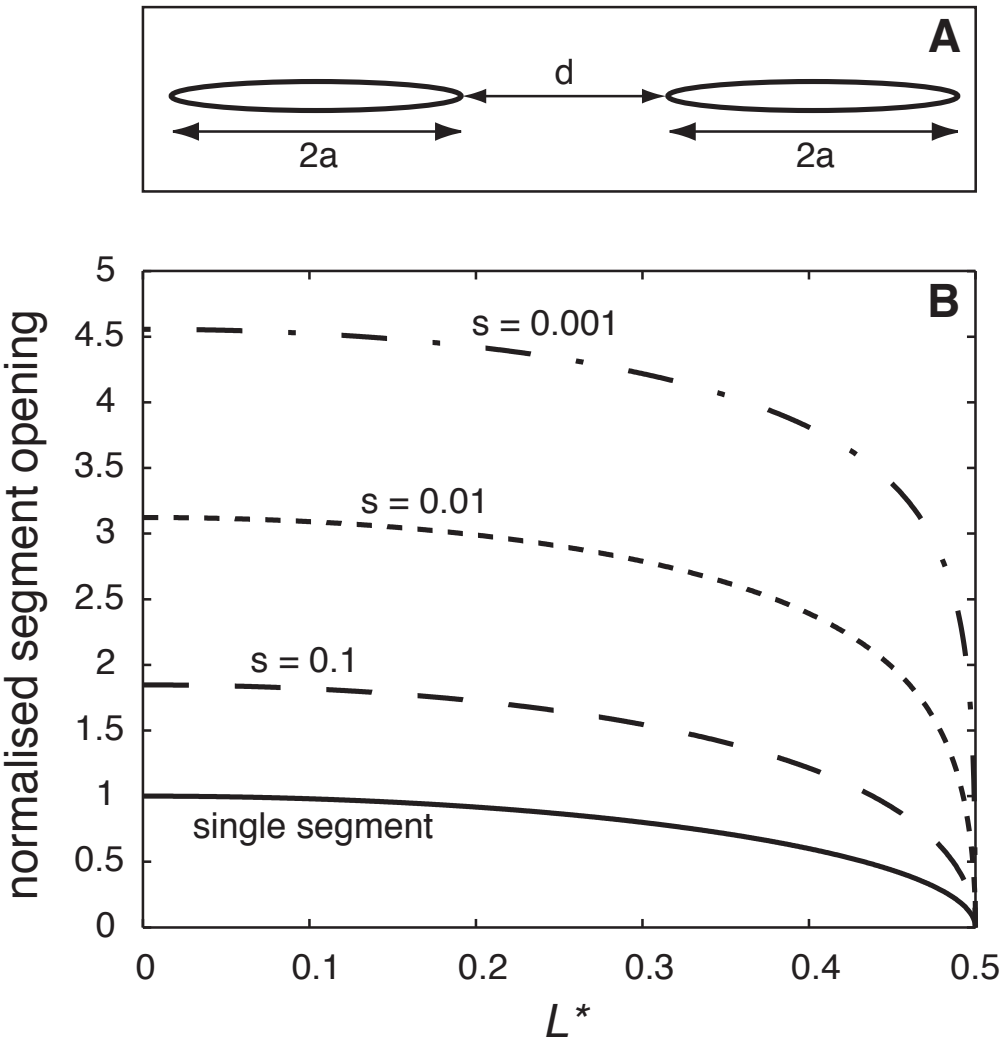

Figure8_Daniels
Click here to download Figure: FIGURE8_Daniels.pdf

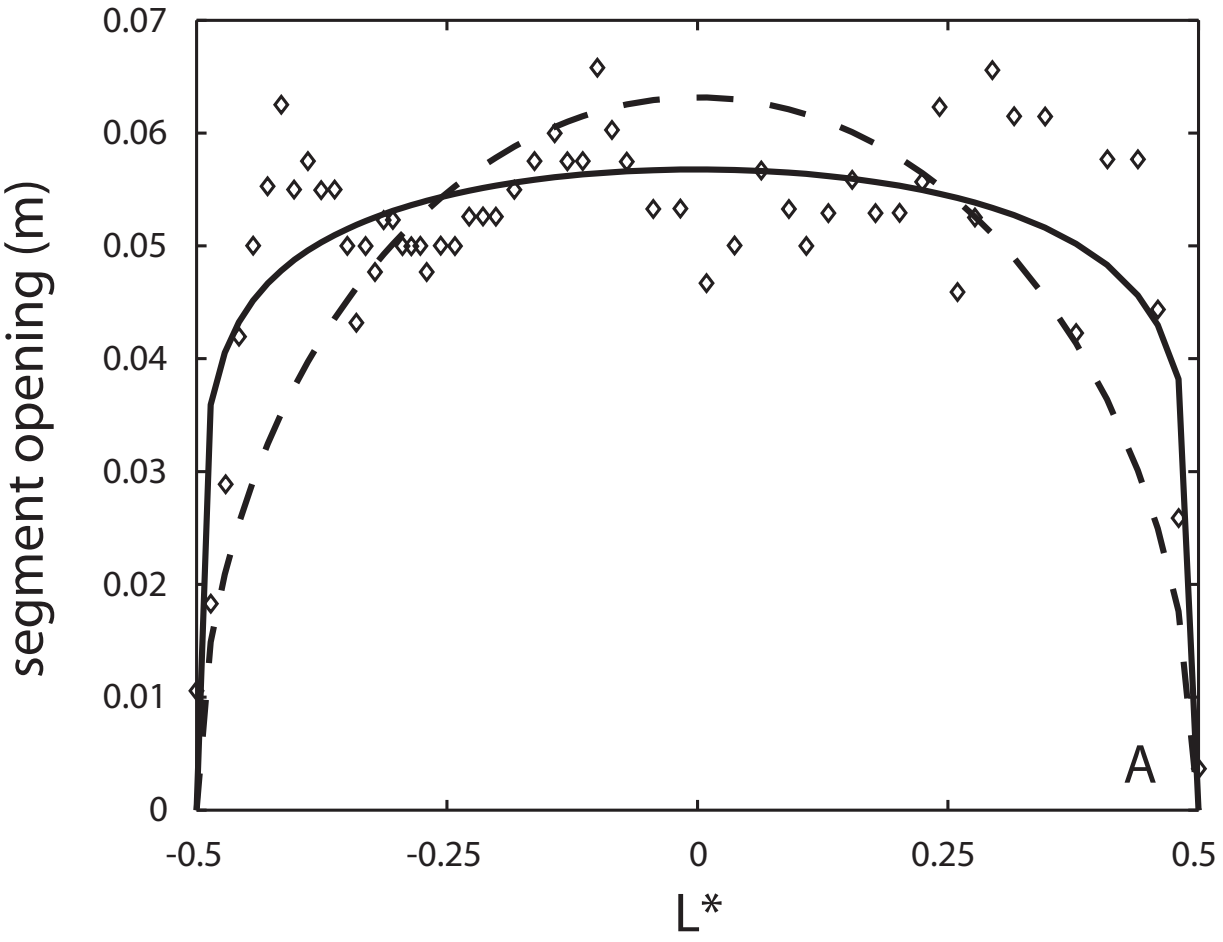

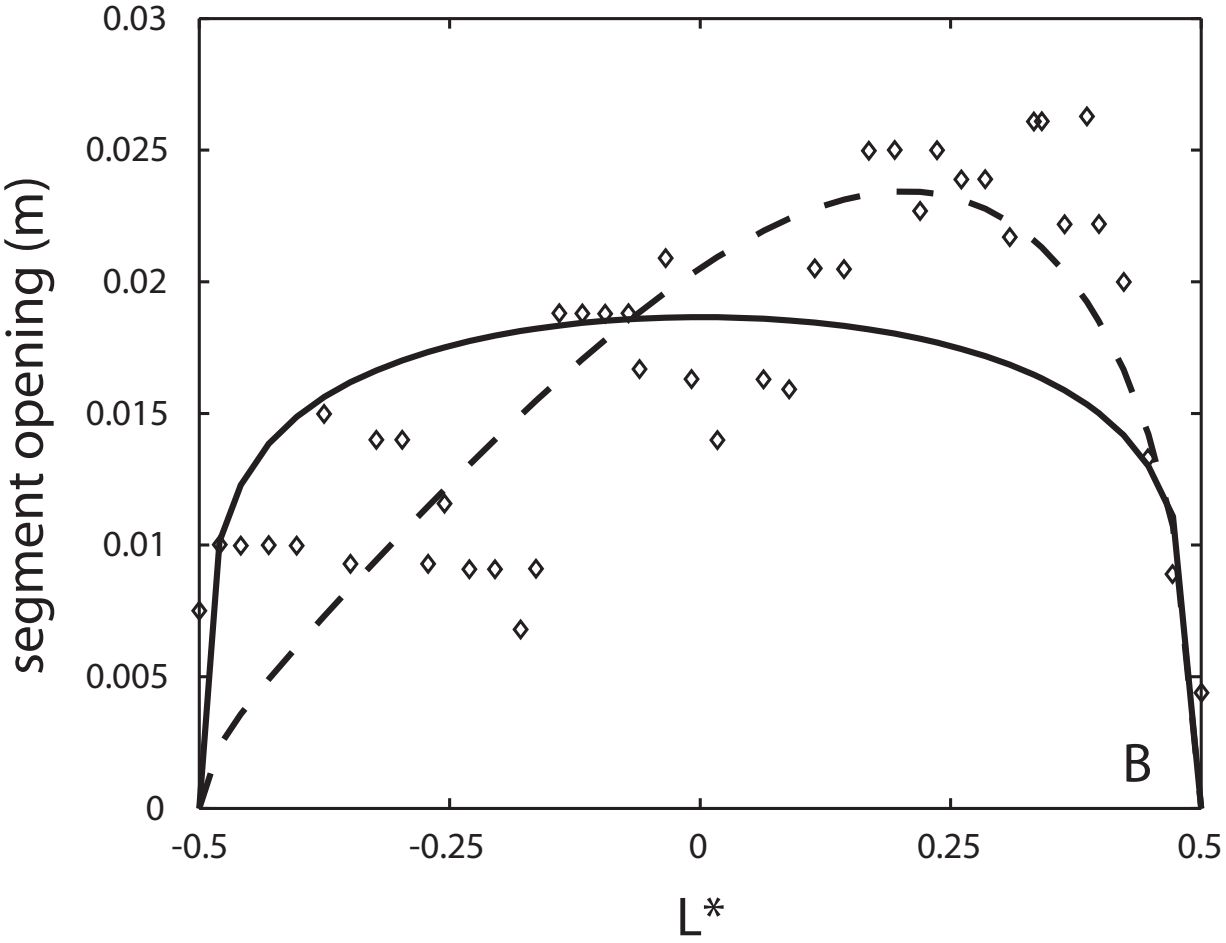

Figure 9 Daniels

Click here to download Figure:

A) Magma-filled fracture

B) Chilled crack tips

C) Solidified magma in fracture